

# High contributions of vehicular emissions to ammonia in three European cities derived from mobile measurements

Miriam Elser<sup>a,1</sup>, Imad El-Haddad<sup>a</sup>, Marek Maasikmets<sup>b,d</sup>, Carlo Bozzetti<sup>a</sup>, Robert Wolf<sup>a</sup>, Giancarlo Ciarelli<sup>a,2</sup>, Jay G. Slowik<sup>a</sup>, Rene Richter<sup>a</sup>, Erik Teinmaa<sup>b</sup>, Christoph Hüglin<sup>c</sup>, Urs Baltensperger<sup>a</sup>, André S.H. Prévôt<sup>a,\*</sup>

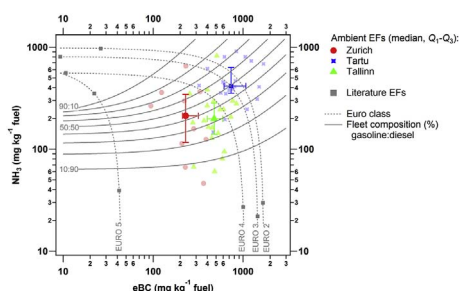
<sup>a</sup> Laboratory of Atmospheric Chemistry, Paul Scherrer Institute, 5232, Villigen PSI, Switzerland

<sup>b</sup> Estonian Environmental Research Centre, 10617, Tallinn, Estonia

<sup>c</sup> Swiss Federal Laboratories for Materials Science and Technology, EMPA, 8600, Dübendorf, Switzerland

<sup>d</sup> Institute of Agricultural and Environmental Sciences, Estonian University of Life Sciences, 51014, Tartu, Estonia

## GRAPHICAL ABSTRACT



## ARTICLE INFO

### Keywords:

Ammonia  
Sources  
Urban  
Traffic  
Emission factors  
Aerosol mass spectrometer

## ABSTRACT

Ambient ammonia ( $\text{NH}_3$ ) measurements were performed with a mobile platform in three European cities: Zurich (Switzerland), Tartu (Estonia) and Tallinn (Estonia) deploying an  $\text{NH}_3$  analyzer based on cavity ring-down spectroscopy. A heated inlet line along with an auxiliary flow was used to minimize  $\text{NH}_3$  adsorption onto the inlet walls. In addition, a detailed characterization of the response and recovery times of the measurement system was used to deconvolve the true  $\text{NH}_3$  signal from the remaining adsorption-induced hysteresis. Parallel measurements with an aerosol mass spectrometer were used to correct the observed  $\text{NH}_3$  for the contribution of ammonium nitrate, which completely evaporated in the heated line at the chosen temperature, in contrast to ammonium sulfate. In this way a quantitative measurement of ambient gaseous  $\text{NH}_3$  was achieved with sufficient time resolution to enable measurement of  $\text{NH}_3$  point sources with a mobile sampling platform. The  $\text{NH}_3$  analyzer and the aerosol mass spectrometer were complemented by an aethalometer and various gas-phase analyzers to enable a complete characterization of the sources of air pollution, including the spatial distributions and the regional background concentrations and urban increments of all measured components. Although at all three locations similar increment levels of organic aerosols were attributed to biomass burning and traffic, traffic emissions clearly dominated the city enhancements of  $\text{NH}_3$ , equivalent black carbon (eBC) and carbon dioxide ( $\text{CO}_2$ ). Urban increments of 3.4, 1.8 and 3.0 ppb of  $\text{NH}_3$  were measured in the traffic areas in Zurich, Tartu and Tallinn, respectively, representing an enhancement of 36.6, 38.3 and 93.8% over the average background

\* Corresponding author.

E-mail address: [andre.prevot@psi.ch](mailto:andre.prevot@psi.ch) (A.S.H. Prévôt).

<sup>1</sup> Present address: Swiss Federal Laboratories for Materials Science and Technology, EMPA, 8600, Dübendorf, Switzerland.

<sup>2</sup> Present address: Laboratoire Inter-Universitaire des Systèmes Atmosphériques (LISA), UMR CNRS 7583, Université Paris Est Créteil et Université Paris Diderot, Institut Pierre Simon Laplace, Créteil, France.

concentrations. Measurements in areas strongly influenced by traffic emissions (including tunnel drives) were used to estimate emission factors (EF) for the traffic-related pollutants. The obtained median EFs range between 136.8–415.1 mg kg<sup>-1</sup> fuel for NH<sub>3</sub>, 157.1–734.8 mg kg<sup>-1</sup> fuel for eBC and 39.9–324.3 mg kg<sup>-1</sup> fuel for HOA. Significant differences were found between the EFs of certain components in the three cities, which were partially linked to an older vehicle fleet in Estonia compared to Switzerland. Using the determined EFs we show that traffic can fully explain the NH<sub>3</sub> enhancements in the three cities and also presents a non-negligible fraction of the background concentrations, which are mostly related to agricultural activities. Moreover, the estimated total contribution of traffic to NH<sub>3</sub> at all three locations is in good agreement with the available emission inventories.

## 1. Introduction

Ammonia (NH<sub>3</sub>) is a major component of the total reactive nitrogen and the predominant gaseous basic compound in the atmosphere. Therefore, NH<sub>3</sub> has major environmental implications, including the eutrophication and acidification of natural ecosystems, which can lead to changes in the species composition (Fangmeir et al., 1994; Krupa, 2003; Bobbink et al., 2010). In the atmosphere, gaseous NH<sub>3</sub> will neutralize sulfuric and nitric acid leading to the formation of ammonium sulfate ((NH<sub>4</sub>)<sub>2</sub>SO<sub>4</sub>), ammonium hydrogen sulfate (NH<sub>4</sub>HSO<sub>4</sub>) and ammonium nitrate (NH<sub>4</sub>NO<sub>3</sub>). These species are the most abundant secondary inorganic compounds in the atmospheric aerosols or PM<sub>2.5</sub> (particulate matter with aerodynamic diameter below 2.5 µm) and thus have significant implications for regional air quality, health effects, visibility, cloud formation and radiative balance. NH<sub>3</sub> can enhance particle nucleation by several orders of magnitude, which affects climate by increasing the number of potential cloud condensation nuclei (Kirkby et al., 2011). The accurate knowledge of NH<sub>3</sub> current atmospheric levels, emission sources and spatial distribution (compared to the pre-industrial era) is fundamental for the assessment of its influence on climate and other ecosystem aspects.

Current estimates of global NH<sub>3</sub> emissions vary between 35 and 65 Tg N year<sup>-1</sup> (Bouwman et al., 1997; Sutton et al., 2013). Combining emission inventories with global models, Sutton et al. (2013) modeled the spatial distributions of NH<sub>3</sub> emissions and reported the dominant sources in each region. NH<sub>3</sub> emissions vary strongly by region, with emission hotspots in China, India, central Africa and northern Europe. In most regions, the dominant NH<sub>3</sub> sources are livestock and crops, while biomass burning is the main NH<sub>3</sub> source across central Africa. However, in urban areas additional anthropogenic sources can be significant. These sources include road traffic, residential coal and biomass burning, industrial NH<sub>3</sub> and fertilizer production, waste management, and human and pets emissions (Sutton et al., 2000; Reche et al., 2012).

NH<sub>3</sub> emissions from gasoline vehicles equipped with a three-way catalyst (TWC) have been shown to be an important source of NH<sub>3</sub> in areas with heavy traffic (e.g. Perrino et al., 2002; Reche et al., 2015). In the TWC, NH<sub>3</sub> is generated as a side product in the NO<sub>x</sub> reduction process (Huai et al., 2003). Remote sensing in London showed a strong increase in traffic-derived NH<sub>3</sub> emission factors (from 520 to 970 mg<sub>NH3</sub> kg<sub>fuel</sub><sup>-1</sup>) when catalyst-equipped vehicles were introduced in the UK fleet in 1992, while since the introduction of Euro 3 vehicles in the year 2000, NH<sub>3</sub> emissions have monotonically decreased, reaching in 2012 similar values to the pre-catalyst times (Carslaw and Rhys-Tyler, 2013). Laboratory dynamometer studies have shown large variability in the EFs of NH<sub>3</sub> for various types of TWC equipped-vehicles, temperatures and driving cycles (e.g. Durbin et al., 2002; Heeb et al., 2006; Huai et al., 2005; Suarez-Bertoa et al., 2014). Furthermore, the recent introduction of the selective catalytic reduction system (SCR) with its addition of urea or NH<sub>3</sub> in heavy-duty vehicles (HDV) and more recently in diesel light-duty vehicles (LDVs) resulted in increased NH<sub>3</sub> emissions from traffic (Suarez-Bertoa and Astorga, 2016), which needs further investigation.

Real-time measurements of NH<sub>3</sub> are hindered by the adsorption of NH<sub>3</sub> on the sampling lines, which severely degrades the measurement time resolution. In this work, we use specially designed inlets and

correction algorithms for a quantitative characterization of NH<sub>3</sub> point sources with a mobile sampling platform in three European cities: Zurich (Switzerland), Tartu (Estonia) and Tallinn (Estonia). Such mobile measurements enabled the characterization of the spatial distribution of NH<sub>3</sub> in the three cities, the determination of NH<sub>3</sub> regional background concentrations and urban increments and the calculation of emission factors (EFs) from specific sources under real world conditions. Traffic EFs were estimated for NH<sub>3</sub>, equivalent black carbon (eBC) and hydrocarbon-like (HOA) and were used to assess the contribution of traffic to the measured NH<sub>3</sub> levels inside the cities.

## 2. Methodologies

### 2.1. Measurement campaigns and instrumentation

Mobile measurements were performed for approximately one week in Zurich (9–19 October 2013), Tartu (10–17 March 2014) and Tallinn (25 March to 1 April 2014). The mobile measurements were mostly performed during daytime, while stationary measurements were additionally performed overnight in Tartu and Tallinn. Driving routes were designed to include different areas of the cities and were covered repeatedly during the measurement campaign (20–30 times) in order to obtain statistically significant spatial distributions of the measured compounds. Meteorological parameters recorded at the NABEL station (Swiss National Air Pollution Monitoring Network) Zurich-Kaserne are reported in Fig. S1.

All details about the mobile laboratory set-up have been reported by Elser et al. (2016) and only a brief description follows. The Paul Scherrer Institute mobile platform (IVECO Turbo Daily Transporter, detailed description in Bukowiecki et al. (2002)) was used as rolling platform for the on-road measurements. An NH<sub>3</sub>-Picarro analyzer (G1103-t) was used to measure real-time NH<sub>3</sub> concentrations. Additionally, the concentrations of CO<sub>2</sub>, CO and CH<sub>4</sub> were measured with a Licor-7000 CO<sub>2</sub>/H<sub>2</sub>O monitor and a Picarro-G2401 CO/CO<sub>2</sub>/CH<sub>4</sub>/H<sub>2</sub>O analyzer (available only in Tartu and Tallinn). Regarding the PM measurements, a high resolution time-of-flight aerosol mass spectrometer (HR-ToF-AMS, Aerodyne Research Inc.) was deployed to investigate the size resolved chemical composition of the non-refractory (NR)-PM<sub>2.5</sub> aerosol (including nitrate (NO<sub>3</sub>), sulfate (SO<sub>4</sub>), ammonium (NH<sub>4</sub>), chloride (Cl), and organic aerosols (OA)). In addition, a seven-wavelength Aethalometer (Magee Scientific, model AE33) was used to measure the light absorption from carbonaceous aerosols and determine the concentrations of equivalent black carbon (eBC) (Drinovec et al., 2015).

The measurement principle of the NH<sub>3</sub>-Picarro analyzer is based on cavity ring-down spectroscopy (CRDS), i.e. the measurement of the absorption of a pulse of light of a specific wavelength trapped in an optical cavity is used to determine the concentration of the absorbing substance in the gas mixture in the cavity. Possible interferences from other gases in the NH<sub>3</sub> quantification are minimized by measuring at reduced pressure, so that absorption line widths are small, and selecting several spectral lines on the basis of its strength and absence of interference from other molecular species (Martin et al., 2016). When interferences are unavoidable, the interfering peaks can be measured and their contributions to the measurement of interest deconvolved and

eliminated. In ambient air, the presence of high and variable water vapor is the primary source of interference in the  $\text{NH}_3$  measurement. Water vapor influences the measurements through the presence of absorption features close to those of  $\text{NH}_3$  and through differences in matrix broadening effects (Martin et al., 2016). Using the water fraction reported by the  $\text{NH}_3$  analyzer and the correction function reported in Martin et al. (2016), we have estimated an average offset in the ammonia concentrations due to the water vapor interference of 0.20 ppb for Zurich, 0.04 ppb for Tartu and 0.03 ppb for Tallinn. This corresponds to an average bias in the ammonia concentrations of 2.5% in Zurich, 1.1% in Tartu, and 1.0% in Tallinn, which we consider to be negligible and has therefore not been corrected for. In addition, possible interferences from other gases including nitrogen oxides and common hydrocarbons have been empirically determined at Picarro Inc. by analyzing the instrument response to mixtures of each interfering gas and dry synthetic air at various concentrations (Table S1). As discussed in Section S2 of the Supplementary material, these interferences are small enough to be negligible at typical ambient conditions. The absence of major interferences in the ambient  $\text{NH}_3$  measurements with the Picarro analyzer is also confirmed by the excellent agreement observed between the online analyzer and two-weekly integrated  $\text{NH}_3$  mini-denuder samples at three different sites in Switzerland over a full year (Fig. S2).

In this work we assess the performance of the  $\text{NH}_3$  Picarro analyzer for real-time mobile measurements, where the main challenge lies in the rapid change in the  $\text{NH}_3$  concentrations. Although the instrument measures with fast time resolution (3 s), the observed response may be significantly delayed by adsorption of  $\text{NH}_3$  onto the inlet walls, often resulting in overall equilibration time scales on the order of minutes to hours. As high time resolution is required to study local sources with the mobile measurements, a new inlet system was tested and used (see Section 3). Moreover, post measurement corrections were applied to

minimize the remaining measurement delays and deconvolve the original  $\text{NH}_3$  signal.

## 2.2. Source apportionment

Positive matrix factorization (PMF, Paatero and Tapper, 1994) was used to identify and quantify the major sources of OA at the three measurement sites. PMF is a bilinear unmixing model which represents the measurements (matrix  $\mathbf{X}$  containing the time series of organic fragments at each  $m/z$ ) as the linear combination of a given number of static factor profiles (in matrix  $\mathbf{F}$ ) and the related time series (in matrix  $\mathbf{G}$ ):

$$\mathbf{X} = \mathbf{G} \times \mathbf{F} + \mathbf{E} \quad (1)$$

where  $\mathbf{E}$  represents the model residuals. The model aims to minimize the object function  $Q$ , defined as the sum of squared model errors ( $e_{ij}$ ) weighted by their respective measurement uncertainties ( $\sigma_{ij}$ ):

$$Q = \sum_i \sum_j \left( \frac{e_{ij}}{\sigma_{ij}} \right)^2 \quad (2)$$

All details about the OA source apportionment strategy using Source Finder (SoFi; Canonaco et al., 2013) are reported in Section S3 of the Supplementary material for Zurich (Figs. S3–S5) and in a previous publication (Elser et al., 2016) for Tartu and Tallinn. In all cases, the four-factor solution was found to represent best the data and the obtained factors were identified as hydrocarbon-like OA (HOA), biomass burning OA (BBOA), cooking OA (COA) or residential-influenced OA (RIOA) and oxygenated OA (OOA). While in Zurich the identification of the COA was supported by the diurnal profiles of such factor, in Estonia the diurnals were more distorted by the mobile nature of the measurements and therefore the influence of other residential emissions (e.g. coal or waste burning) couldn't be excluded.

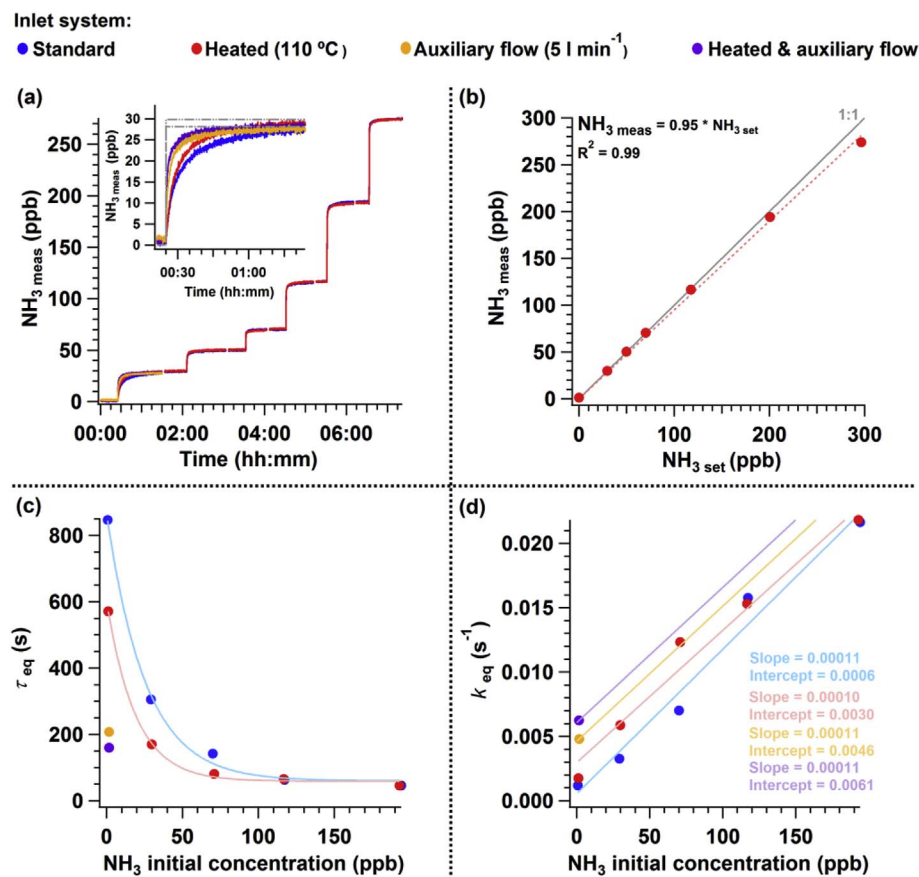


Fig. 1. Laboratory calibrations of the  $\text{NH}_3$  analyzer using different inlet systems. (a) System (inlet plus analyzer) response time at different concentration ranges. (b) Concentration calibration curve, fitted with a linear function. (c) Equilibration time ( $\tau_{eq}$ ) of the system for the concentration ranges shown in (a), fitted with exponential functions. (d)  $k_{eq}$  ( $k_{eq} = \tau_{eq}^{-1}$ ) for the concentration ranges shown in (a), fitted with linear functions. The average slope determined for the calibrations without an auxiliary flow was used to fit the calibrations with the auxiliary flow (for which only one point is available).

The Aethalometer model described in Sandradewi et al. (2008) was used for the source apportionment of eBC. This method exploits the enhanced absorption of wood burning particles in the ultraviolet and visible wavelengths region relative to that of traffic particles to separate the contributions of these sources (denoted  $eBC_{wb}$  and  $eBC_{tr}$ , respectively). The absorption measured at 470 and 950 nm was used to calculate the Ångström exponent and, following the suggestions in Zotter et al. (2017), Ångström exponents of 0.9 and 1.7 were used for traffic and wood burning, respectively. For a correct separation of the two fractions, the Aethalometer data was averaged to 30 min in order to increase the signal to noise ratio. Therefore, the resulting eBC fractions could only be used for the study of the correlations with the sources of OA, but not for the study of point sources or spatial distributions.

### 3. Optimization of the $NH_3$ sampling system and deconvolution of the $NH_3$ signal

The high water solubility and polarity of  $NH_3$  causes significant adsorption onto sampling line surfaces, severely degrading measurement time resolution. Without specially designed inlets and/or correction algorithms, these time delays are often large enough to prevent quantitative measurements from mobile platforms, let alone source resolution. To minimize this effect,  $NH_3$  was sampled through a 4 mm I.D., 1 m long PTFE inlet line heated to 110 °C (to decrease the net adsorption) along with an auxiliary flow of 5 l min<sup>-1</sup> (to decrease the residence time in the line).

Fig. 1 illustrates laboratory calibrations of the system response time using different inlet systems: standard line (PTFE, I.D. 4 mm, L 1 m), heated line (standard inlet at  $T = 110$  °C), auxiliary flow (standard inlet with  $F_{aux} = 5$  l min<sup>-1</sup>), and heated line with auxiliary flow (standard inlet at  $T = 110$  °C and with  $F_{aux} = 5$  l min<sup>-1</sup>). Different concentrations of  $NH_3$  ( $NH_{3, set}$ ) were generated with a calibrated permeation tube and injected stepwise in the sampling system until equilibrium was reached (Fig. 1a). The measurement of  $NH_3$  is very precise and accurate ( $NH_{3, meas}/NH_{3, set} = 0.95$ , with  $R^2 = 0.99$ ) over a wide range of concentrations (Fig. 1b). However, a substantial adsorption-induced delay is still observed in the  $NH_3$  response time, especially at low concentrations. Heating the inlet line and adding an auxiliary flow

significantly reduce the time required to reach equilibrium.

The equilibration of  $NH_3$  on the tube walls can be described by a Langmuir-type process, where the quantity of the adsorbed  $NH_3$  depends on the surface/ $NH_3$  thermodynamics (e.g. number of available sites), which is driven by the concentration of gaseous  $NH_3$  and the tube temperature. The equilibration profile of the measured  $NH_3$  ( $NH_{3, meas}$ ), i.e. the transition from the perturbed state to the new equilibrium state, follows second order kinetics with respect to the  $NH_3$  surface concentration. The dynamic response of  $NH_{3, meas}$  under these conditions has the form of a double exponential function:

$$\frac{NH_{3, meas}}{NH_{3, set}} = 1 + A_1 \times e^{-\frac{t}{\tau_1}} + (1 - A_1) \times e^{-\frac{t}{\tau_2}} \quad (3)$$

Here,  $t$  is the time elapsed after perturbation (change in  $NH_{3, set}$  concentration), and  $\tau_1$  and  $\tau_2$  represent the equilibration times weighted by the exponential pre-factors  $A_1$  and  $(1 - A_1)$ , respectively.

During mobile sampling, changes in  $NH_3$  concentrations are very rapid and typically constrained to a limited range. Consequently, these changes are not expected to induce a large perturbation in the adsorbed  $NH_3$  surface concentration. As such, the dynamic response of gaseous  $NH_3$  concentrations in the tube does not significantly depend on the amount of  $NH_3$  adsorbed, and can therefore be approximated by a pseudo-first order process. Such a process can be represented based on the balance of  $NH_3$  molecular flows in the tube, assuming that any difference between the measured and set  $NH_3$  concentrations beyond the gas residence time in the inlet line (negligible) is related to the adsorption of  $NH_3$  onto the inlet surface:

$$\frac{dNH_3}{dt} = k_{eq} \times NH_{3, set} - k_{eq} \times NH_{3, meas} \quad (4)$$

In this expression,  $k_{eq}$  is the first-order equilibration rate of  $NH_3$  in the inlet line. Equilibration rates and time scales ( $\tau_{eq} = k_{eq}^{-1}$ ) were calculated at different temperatures, inlet flows and  $NH_3$  concentrations (Fig. 1c and d), from the weighted average of  $\tau_1$  and  $\tau_2$  determined from our calibration data (Fig. 1a) using Eq. (3).  $k_{eq}$  shows the expected linear increase against the  $NH_3$  concentrations. In the range of ambient concentrations a minor change in these rates, below a factor two, can be anticipated. The  $NH_3$  equilibration time was significantly minimized by

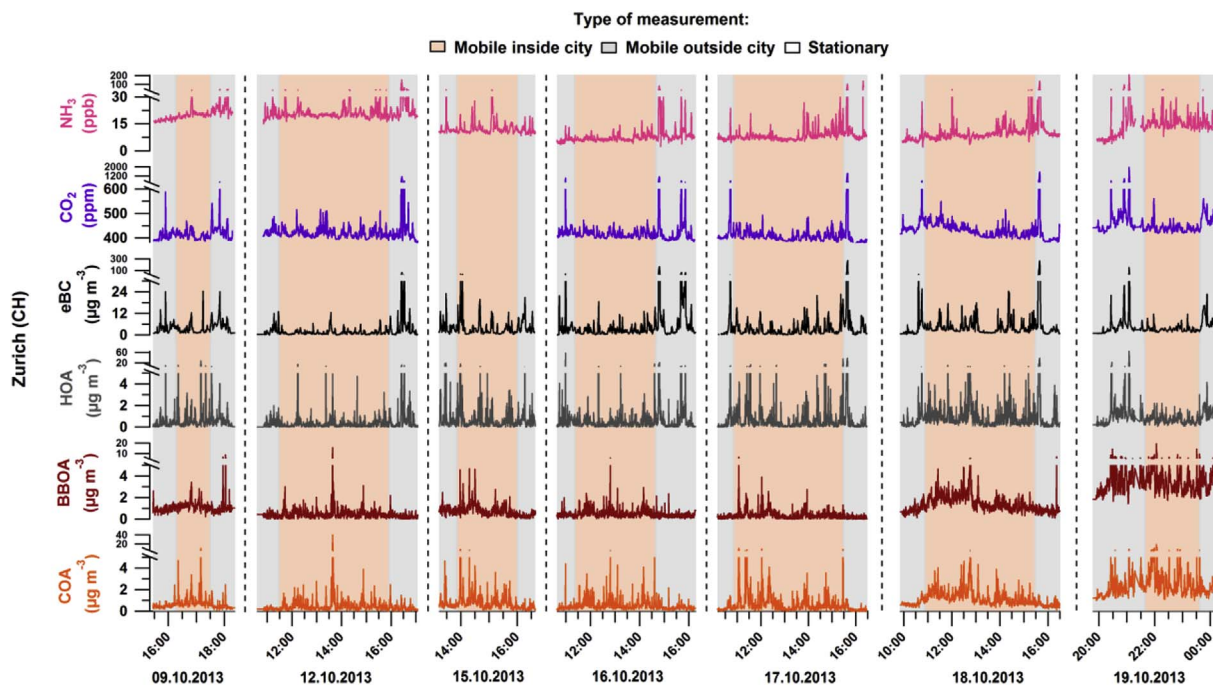


Fig. 2. Time series of ammonia ( $NH_3$ ), carbon dioxide ( $CO_2$ ), equivalent black carbon (eBC), hydrocarbon-like organic aerosol (HOA), biomass burning organic aerosol (BBOA) and cooking organic aerosol (COA) for the measurements in Zurich.

heating the inlet to 110 °C (decrease in  $\tau_{eq}$  by a factor of 1.5) and by adding an auxiliary flow of 5 l min<sup>-1</sup> (decrease in  $\tau_{eq}$  by a factor of 4.1). These improved settings are then used for the measurements of NH<sub>3</sub> in ambient air.

Despite these improvements, delays in ambient NH<sub>3</sub> signals were still observed. This is illustrated in Fig. S6 for the case of traffic-related

emissions during tunnel drives in Zurich, where the measured NH<sub>3</sub> signal exhibited delayed and broader peaks compared to the other traffic tracers. By rearranging Eq. (4) and using the concentration dependent equilibration rates determined experimentally, the measured NH<sub>3</sub> signal (NH<sub>3</sub> meas) was deconvolved to estimate the real NH<sub>3</sub> concentration in the atmosphere (NH<sub>3</sub> set or NH<sub>3</sub> deconvolved):

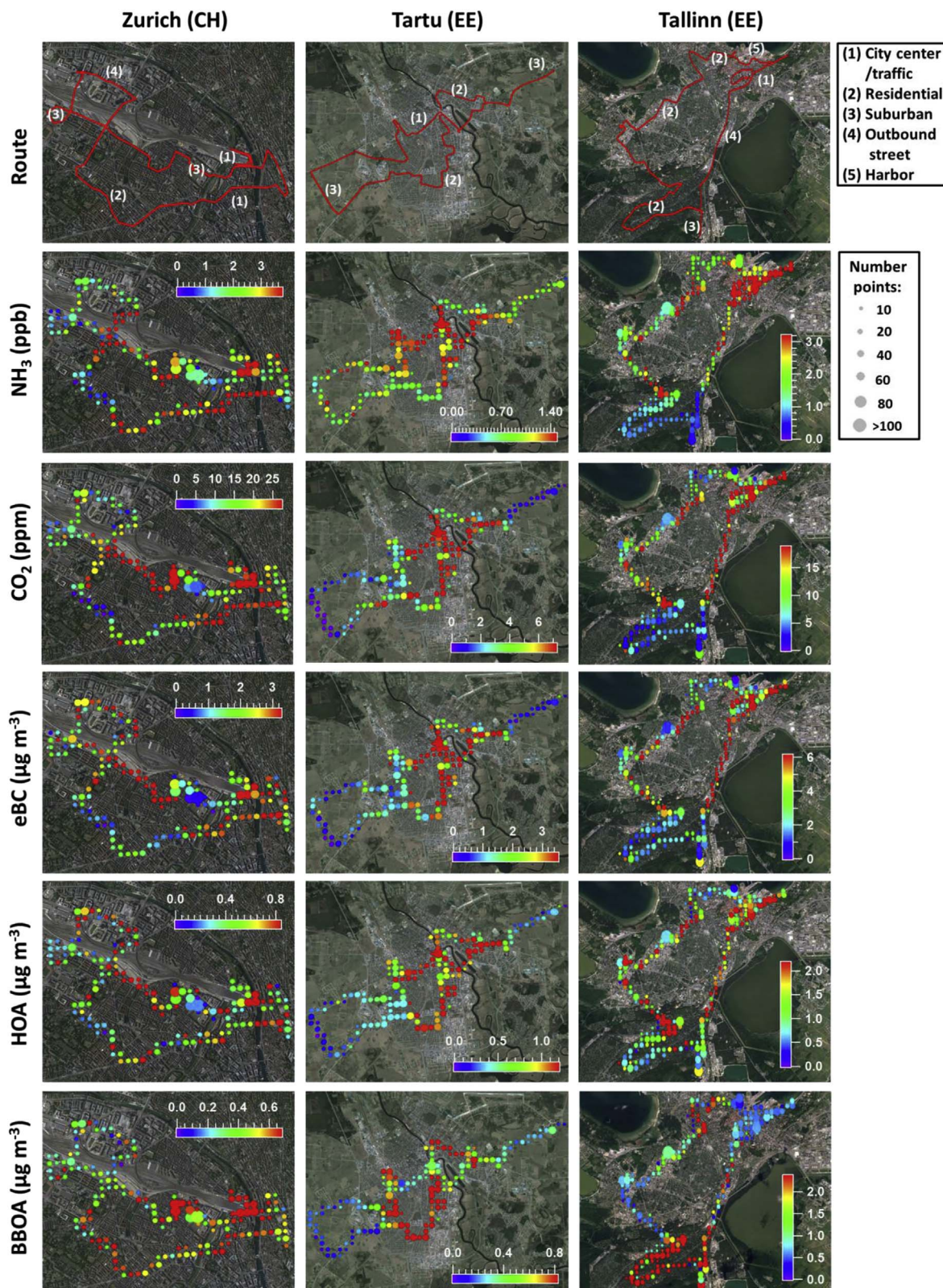


Fig. 3. Spatial distributions of the enhancements (over the background concentrations) of NH<sub>3</sub>, CO<sub>2</sub>, eBC, HOA and BBOA at the three measurement locations.

$$\text{NH}_3_{\text{set}} = \frac{\frac{d\text{NH}_3}{dt} + k_{\text{eq}}(\text{NH}_3_{\text{meas}}) \times \text{NH}_3_{\text{meas}}}{k_{\text{eq}}(\text{NH}_3_{\text{meas}})} \quad (5)$$

The dependence of  $k_{\text{eq}}$  on the  $\text{NH}_3$  concentration was derived from calibrations conducted without an auxiliary flow. The example shown in Fig. S6 illustrates that this correction significantly improves the agreement between  $\text{NH}_3_{\text{deconvolved}}$  and other pollutants concomitantly emitted in the tunnels. In all cases the correlation coefficients are significantly higher after the correction is applied, i.e.  $R^2$  for  $\text{NH}_3$  vs. eBC increased from 0.32 to 0.41, for  $\text{NH}_3$  vs.  $\text{CO}_2$  from 0.55 to 0.78 and for  $\text{NH}_3$  vs. HOA from 0.35 to 0.60 (Table S2). Note that if the standard inlet set-up (without heating and auxiliary flow) had been deployed, many peaks of  $\text{NH}_3$  at ambient relevant concentrations would not have been detected and the deconvolution of the signal would not have been possible. Moreover, although the deconvolution algorithm amplifies the measurement noise, the mean error introduced in this way is only important at very low concentrations and decreases to a few percent at concentrations above 30 ppb (Fig. S7).

Another potentially important issue encountered during the measurement of gaseous  $\text{NH}_3$  is the interference from particulate ammonium. At 110 °C, ammonium salts present in the atmosphere (mainly  $\text{NH}_4\text{NO}_3$  and  $(\text{NH}_4)_2\text{SO}_4$ ), can volatilize in the inlet line creating a positive artifact in the  $\text{NH}_3$  measurement. Here, we take advantage of the AMS to estimate the concentration of  $\text{NH}_3$  derived from the particle phase. Laboratory tests showed that under the above conditions  $\text{NH}_4\text{NO}_3$  fully evaporates in the heated line, whereas all the  $(\text{NH}_4)_2\text{SO}_4$  remains in the particle phase (see Fig. S8). Accordingly, the measured  $\text{NH}_3$  concentrations represent the aggregate of gas phase  $\text{NH}_3$  and particle phase  $\text{NH}_4\text{NO}_3$ . Ambient  $\text{NH}_3$  concentrations were corrected by subtracting the  $\text{NH}_3$  corresponding to the  $\text{NH}_4\text{NO}_3$  measured with the AMS. At all three locations the gas phase  $\text{NH}_3$  dominated over the particulate fraction, i.e.  $\text{NH}_3_{\text{gas}}/\text{NH}_3_{\text{gas} + \text{particle}}$  of 0.98 (0.92; 0.99) (median ( $Q_1$ ;  $Q_3$ )), 0.97 (0.80; 0.99) and 0.94 (0.79; 0.99) were obtained for Zurich, Tartu and Tallinn, respectively.

## 4. Results and discussion

### 4.1. Temporal variability of $\text{NH}_3$

The temporal evolution of  $\text{NH}_3$  and other primary pollutants including  $\text{CO}_2$ , CO (available only for the measurements conducted in Estonia), eBC, HOA, BBOA and COA or RIOA are shown in Fig. 2 for Zurich and in Fig. S9 for Estonia. The time series of the additional measured components and sources are reported in Fig. S10 for Zurich and in a previous publication for Tartu and Tallinn (Elser et al., 2016). The  $\text{NH}_3$  background concentrations show a considerable day-to-day variability, consistent with that of regional pollutants such as secondary aerosols ( $\text{SO}_4$ ,  $\text{NO}_3$ ,  $\text{NH}_4$ , and OOA) and of  $\text{CO}_2$ . During the city measurements,  $\text{NH}_3$  background concentrations (defined here as the 5th percentile ( $P_{05}$ ) of the concentrations for each round of measurements) ranged between 5 and 19 ppb in Zurich, 2–10 ppb in Tartu and 2–5 ppb in Tallinn. The higher  $\text{NH}_3$  background concentrations detected in Zurich compared to Tartu and Tallinn might be related to the more intense agricultural activity in Switzerland, although effects from different meteorological conditions or differences in the specific agricultural activities ongoing in the different measurement periods also need to be considered. Discrete events with  $\text{NH}_3$  concentrations reaching approximately 50 ppb were observed in all three cities, while peaks up to 200 ppb were measured during tunnel drives in Zurich.

### 4.2. Spatial distributions and urban increments

The spatial distributions of the measured compounds were calculated for the three measurement locations as described in Elser et al. (2016), and only a brief description is given here. The enhancement of each species of interest over its background concentrations was

determined by subtracting the 5th percentile ( $P_{05}$ ) of its concentration during the single loops. The enhancement time series of each compound was then averaged over a spatial grid with grid cells of 100 m<sup>2</sup> in Zurich and 250 m<sup>2</sup> in Tartu and Tallinn. Fig. 3 shows the average spatial distribution of the combustion related compounds, including  $\text{NH}_3$ ,  $\text{CO}_2$ , eBC, HOA and BBOA, at the three measurement locations. The color scale indicates the average enhancement (with the maximum of the scale set to the 75th percentile for better visualization), and the point size represents the number of measurement points that were averaged. The spatial distributions of all other measured components can be found in Fig. S11 (Zurich) and in Elser et al. (2016) (Tartu and Tallinn).

At all three locations, the spatial distributions of  $\text{NH}_3$ ,  $\text{CO}_2$  and eBC are consistent with the distribution of HOA, showing higher enhancements in the city center and areas with elevated traffic. Relatively high correlations are observed between these traffic-related components, with  $R^2$  ranging between 0.25 and 0.82 for the individual cities (Fig. S12). In contrast, the spatial distribution of BBOA is significantly different (especially in Tartu and Tallinn), with higher enhancements observed in residential areas. In the traffic areas of Zurich,  $\text{NH}_3$  shows enhancements ( $P_{75} - P_{05}$ ) of 3.4 ppb over an average background concentration ( $P_{05}$ ) of 9.3 ppb, which represents an increase of about 36.6% (Fig. S13). A similar relative increase in  $\text{NH}_3$  was observed in the areas influenced by traffic in Tartu, with enhancements ( $P_{75} - P_{05}$ ) of 1.8 ppb over an average background concentration of 4.7 ppb (i.e. an increase of 38.3%), while in Tallinn  $\text{NH}_3$  was up to 93.8% higher in the traffic areas of the city due to both high enhancements ( $P_{75} - P_{05}$  of 3.0 ppb) and lower background concentrations (3.2 ppb, on average).

An alternative way to determine the regional background concentrations and the urban increments is to use the longitude profiles as defined by Lenschow et al. (2001) and described in Elser et al. (2016). Such analysis could only be performed for Tartu, as no proper regional background areas were included in the routes in Tallinn and Zurich. The longitude profile of the  $\text{NH}_3$  enhancement in Tartu was obtained by averaging the enhancements in longitude bins (see Fig. S14) and was fitted with a sigmoid function to determine regional background concentrations of 5.1 ppb (average) and 5.4 ppb (median), and urban increments of 0.6 ppb (average) and 0.3 ppb (median), i.e. an increase of 12% (average) and 6% (median) in  $\text{NH}_3$  within the full city area of Tartu (see Table S3).

Note that although at all three locations the measured levels of HOA and BBOA were comparable (enhancement ( $P_{75} - P_{05}$ ) of 0.84  $\mu\text{g m}^{-3}$  HOA and 0.68  $\mu\text{g m}^{-3}$  BBOA in Zurich, 1.17  $\mu\text{g m}^{-3}$  HOA and 0.82  $\mu\text{g m}^{-3}$  BBOA in Tartu, and 2.17  $\mu\text{g m}^{-3}$  HOA and 2.37  $\mu\text{g m}^{-3}$  BBOA in Tallinn), the spatial distributions and their correlations (Fig. 3 and S12) suggest that traffic dominates the enhancements of  $\text{NH}_3$ ,  $\text{CO}_2$  and eBC. This is also supported by Fig. S15, which shows that biomass burning emissions didn't significantly influence the levels of  $\text{NH}_3$ ,  $\text{CO}_2$  and eBC.

### 4.3. Traffic emission factors

Mobile measurements are uniquely suited for the estimation of pollutant emission factors from specific point or line sources, e.g. traffic, under real world conditions. Although many test bench studies report detailed vehicular emissions, the number of tested vehicles is often limited and laboratory/driving conditions strongly influence the results.

The tunnel drives in Zurich allowed for the calculation of traffic emission profiles for  $\text{NH}_3$ , eBC and HOA, under the reasonable assumption that the enhancements inside the tunnel are due to traffic emissions. Similarly to the effect of the inlet line, the adsorption of  $\text{NH}_3$  on the tunnel surface may cause a delay in the  $\text{NH}_3$  concentration rise and fall, influencing the determination of the tunnel  $\text{NH}_3$  EF. However, as discussed in Section S8 of the Supplementary material, this delay does not seem to be substantial compared to the variability in the EFs and can be neglected. The EFs were calculated by integrating the area

below the peaks observed in the traffic-related pollutants when driving through the tunnels (see Fig. S6) as follows:

$$EF = \frac{\int (C_i - C_{i,0})}{\int (C_{CO_2} - C_{CO_2,0})} \times \frac{MW_{CO_2}}{MW_C} \times w_c, \text{ with } i = \text{NH}_3, \text{ eBC and HOA} \quad (6)$$

where the subscript 0 indicates the background concentrations measured at the entrance of the tunnel,  $MW_{CO_2}$  and  $MW_C$  are the molecular weights of  $CO_2$  and carbon, and  $w_c = 0.85$  is the mass fraction of carbon in gasoline (or diesel) fuel. The integration area extends from the rising edge of the peak (where the background concentrations are assigned) until the peak tail reaches again the background levels. Five different tunnels were included in the calculation of the tunnel-based EFs in Zurich. While these comprise highway and city tunnels of variable lengths (400–3300 m) and variable average speeds from 30 to 90 km h<sup>-1</sup>, no trend was observed in the estimated EFs with the different measurement conditions.

Similarly, event-based traffic EFs were estimated for all three locations by integrating traffic-related peaks during the city drives. Periods with high concentrations of  $NH_3$ ,  $CO_2$ , eBC and HOA (above  $P_{25}$ ) and low concentrations of BBOA (below  $P_{50}$ ) were considered for the selection of the events used for the calculation of the EFs (see Fig. S18). As for the tunnel measurements, the background concentrations were subtracted prior to the integration of the peaks in order to exclude the influence of sources other than traffic. A total of twenty traffic events were separated for Tartu and Tallinn, while only ten clear traffic peaks were distinguished in Zurich.

The mean values and the variability of the tunnel-based and event-based traffic EFs are represented as box-and-whiskers in Fig. 4 and reported in Table S4 in the Supplementary material. The estimated EFs reflect the high variability in real world traffic emission factors, as already observed in previous ambient and test bench studies (e.g. Carslaw and Rhys-Tyler, 2013; Suarez-Bertoa et al., 2014). Table 1 presents the results of unpaired Mann-Whitney tests on the distributions of the EFs reported in Fig. 4. No significant differences (i.e.  $p$ -value > 0.025) are observed between the EFs estimated in Zurich using the tunnel-based and event-based methods, which indicates that the uncertainties in both methods are lower than the variability of the EFs. In contrast, clear differences can be seen between the event-based EFs in the three cities, especially for eBC and HOA. The median  $NH_3$  EFs estimated for Zurich

**Table 1**

$p$ -values from unpaired (two sample) Mann-Whitney tests between the distributions of the EFs obtained from the tunnel measurements in Zurich and the city measurements in Zurich, Tartu and Tallinn. The numbers in grey indicate no significant difference (i.e.  $p$ -value > 0.025).

$p$ -value	Tunnels vs. Zurich	Zurich vs. Tartu	Zurich vs. Tallinn	Tartu vs. Tallinn
$NH_3$	0.26	3.7·10 <sup>-3</sup>	1.0	7.8·10 <sup>-5</sup>
eBC	0.57	2.0·10 <sup>-5</sup>	1.3·10 <sup>-4</sup>	4.8·10 <sup>-4</sup>
HOA	0.89	1.6·10 <sup>-5</sup>	2.4·10 <sup>-5</sup>	8.8·10 <sup>-4</sup>

and Tallinn are fairly similar (212 and 199 mg kg<sup>-1</sup> fuel, respectively), and no significant difference was found between their distributions. In comparison, the  $NH_3$  EF was estimated to be a factor of two higher in Tartu (415 mg kg<sup>-1</sup> fuel), which represents a clear difference relative to Zurich and Tallinn (Mann-Whitney test on  $NH_3$  distributions;  $p_{\text{Zurich-Tartu}} = 3.7 \cdot 10^{-3}$  and  $p_{\text{Tartu-Tallinn}} = 7.8 \cdot 10^{-5}$ ). The EFs estimated for eBC are always similar or higher to those of  $NH_3$ . The lowest eBC EF was estimated for Zurich (230 mg kg<sup>-1</sup> fuel), followed by Tallinn (476 mg kg<sup>-1</sup> fuel) and Tartu (735 mg kg<sup>-1</sup> fuel). The Mann-Whitney test results confirm the significance of these differences (Mann-Whitney test on eBC distributions;  $p_{\text{Zurich-Tartu}} = 2.0 \cdot 10^{-5}$ ,  $p_{\text{Zurich-Tallinn}} = 1.3 \cdot 10^{-4}$ ,  $p_{\text{Tartu-Tallinn}} = 4.8 \cdot 10^{-4}$ ). Significant differences were also found among the distributions of the HOA EFs in the three cities (Mann-Whitney test on HOA distributions;  $p_{\text{Zurich-Tartu}} = 1.6 \cdot 10^{-5}$ ,  $p_{\text{Zurich-Tallinn}} = 2.4 \cdot 10^{-5}$ ,  $p_{\text{Tartu-Tallinn}} = 8.8 \cdot 10^{-4}$ ), with a much lower EF estimated for Zurich (40 mg kg<sup>-1</sup> fuel) compared to Tallinn (137 mg kg<sup>-1</sup> fuel) and Tartu (324 mg kg<sup>-1</sup> fuel). These observed differences will be explained in detail below.

To investigate differences in the vehicular fleets at the three measurement locations, Fig. 5 displays the event-based EFs of  $NH_3$  against those of eBC. The reported  $NH_3$ -eBC isopleths for the different Euro classes and gasoline:diesel shares were determined using literature average EFs for gasoline and diesel vehicles for each Euro-class. Despite the large scatter in the EFs, clear trends can be observed in the median EFs for Zurich, Tartu and Tallinn. The estimated gasoline:diesel share shows a certain variability among the three cities, gasoline vehicles representing around 44% of the total fleet in Zurich, 49% in Tartu and 33% in Tallinn. However, a wider spread is observed in the  $NH_3$  EFs

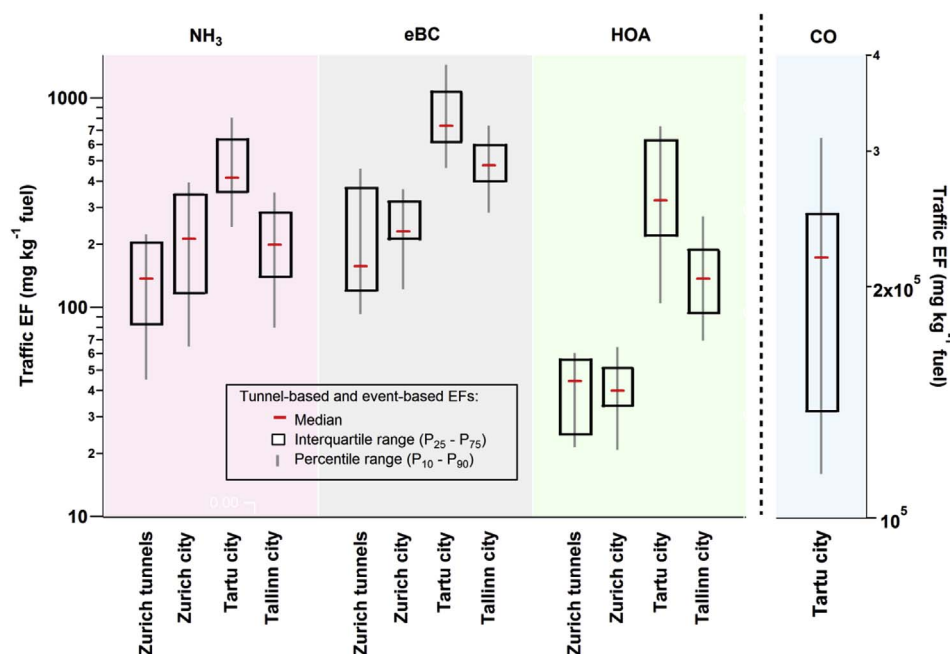


**Fig. 4.**  $NH_3$ , eBC, HOA and CO traffic emission factors calculated from tunnel drives in Zurich (tunnel-based) and from city measurements in Zurich, Tartu and Tallinn (event-based).

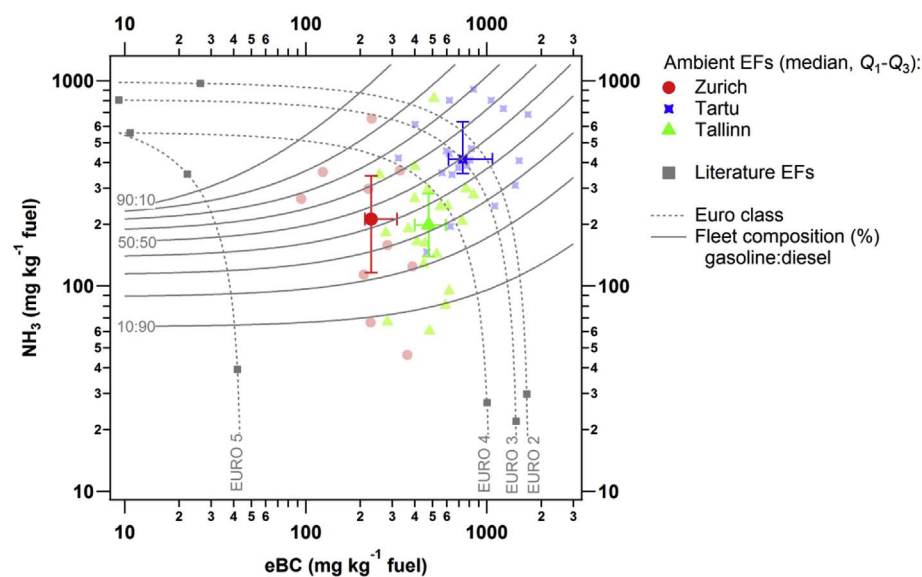


Fig. 5. EFs of  $\text{NH}_3$  versus eBC (points in light colours from event-based analyses; median and interquartile range highlighted) for the three measurement locations. The  $\text{NH}_3$ -eBC isopleths for the different EURO classes were determined fitting a linear function between the literature average EFs for gasoline and diesel vehicles for each EURO class (André et al., 2006; Alves et al., 2013, 2015; Carslaw and Rhys-Tyler, 2013; Huang et al., 2013; Lopes et al., 2014; May et al., 2014). The same literature EFs were used to determine the isopleths for the fleet composition, which were also fitted with a linear function. (For interpretation of the references to colour in this figure legend, the reader is referred to the web version of this article.)

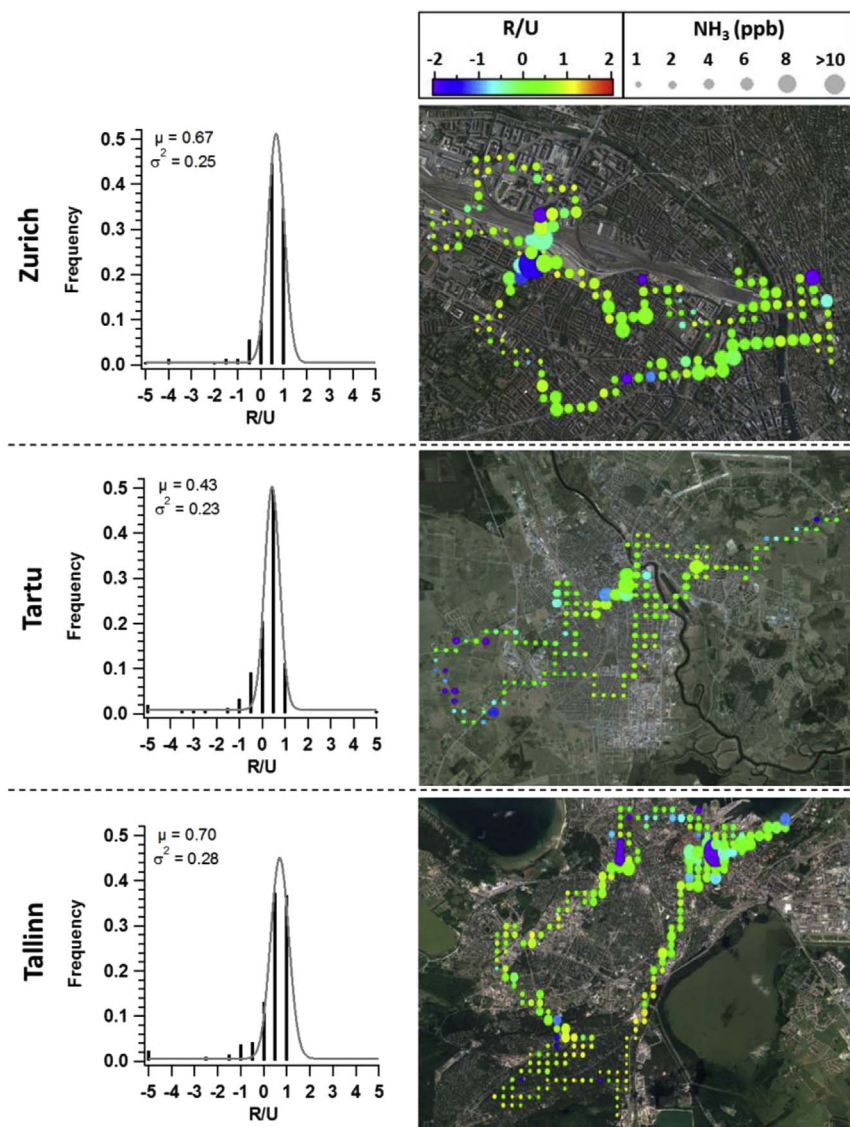


Fig. 6. Frequency and spatial distributions of the residuals to uncertainty ratios (R/U) from the fit of  $\text{NH}_3$  with HOA and the traffic EFs for the three measurement locations.

calculated for each city, suggesting a large variability in the gasoline:diesel shares. This is somehow expected given the different spatial distributions of light and heavy duty vehicles within the same city. Meanwhile clear differences in the eBC EFs between the different cities suggest a significant difference between the average fleet age in Zurich (between EURO 4 and EURO 5), Tallinn (slightly higher than EURO 4) and Tartu (EURO 3). This difference is consistent with fuel consumption data by the different vehicle shares in Switzerland and in Estonia, indicating a higher contribution of EURO 3 vehicles in Estonia (Fig. S19).

While  $\text{NH}_3$  is mostly emitted from the gasoline vehicles equipped with a TWC, eBC and HOA are dominated by the emissions of old diesel vehicles not equipped with a diesel particulate filter (DPF). As shown by Carslaw and Rhys-Tyler (2013), since the introduction of the EURO 3 the  $\text{NH}_3$  emissions from the TWC gasoline vehicles have decreased linearly with the manufacturing year of the car. In contrast to this gradual decrease in the  $\text{NH}_3$  emissions, the emissions of eBC and HOA from diesel vehicles got sharply reduced with the introduction of the DPF (Euro 5). Thus, the higher share of emissions from EURO 3 vehicles in Estonia compared to Switzerland can explain the large difference in the HOA and eBC EFs for the two countries, as well as the much lower difference in the  $\text{NH}_3$  EFs. The differences in the EFs estimated for the two Estonian cities can also partially be related to differences in the car fleet age in these two cities. In fact, as shown in Fig. S20, the fleet in Harju county (which includes Tallinn) is characterized by newer vehicles compared to Tartu county. Considering this county level data (which includes only cars), we estimated an average EURO 2.3 for Tartu county and EURO 2.9 for Harju county. However, our results for Tartu and Tallinn show larger differences, which are probably related to the measurement of a higher fraction of diesel vehicles in Tallinn, where the driving route included an outbound road with high density of diesel trucks. Indeed, the EFs estimated for Tallinn show a lower gasoline:diesel share (33%:67%) compared to Tartu (49%:51%), an indication that our average EFs obtained for Tallinn seem to be slightly biased by higher diesel emissions.

#### 4.4. Traffic contribution to measured $\text{NH}_3$ and comparison with emission inventories

As previously stated, the analyses of the spatial distributions and their correlations indicate that traffic may dominate  $\text{NH}_3$  enhancements within the three cities. We estimated the contribution of traffic related  $\text{NH}_3$  ( $\text{NH}_3_{\text{fit}}$ ), by considering HOA as our best available traffic tracer and the average emission ratio of  $\text{NH}_3$  to HOA ( $ER_{(\text{NH}_3, \text{HOA})}$ ) from the event-based analyses. We compare the estimated traffic related  $\text{NH}_3$  ( $\text{NH}_3_{\text{fit}}$ ) to the total measured  $\text{NH}_3$  ( $\text{NH}_3_{\text{meas}}$ ) by means of the residual to uncertainty ratio ( $R/U$ ):

$$\frac{R}{U} = \frac{\text{NH}_3_{\text{fit}} - \text{NH}_3_{\text{meas}}}{\sigma_{\text{NH}_3_{\text{fit}}}} = \frac{ER_{(\text{NH}_3, \text{HOA})} \times \text{HOA} - \text{NH}_3_{\text{meas}}}{\sigma_{ER_{(\text{NH}_3, \text{HOA})}} \times \text{HOA}}, \quad (7)$$

where  $\sigma_{\text{NH}_3_{\text{fit}}}$  is the standard deviation of the fitted  $\text{NH}_3$  traffic contribution and is given by the product of the standard deviation of the event-based ER ( $\sigma_{ER_{(\text{NH}_3, \text{HOA})}}$ ) and HOA. The frequency and spatial distributions of  $R/U$  are reported in Fig. 6 for the three measurement locations. In all cases, the frequency distributions of  $R/U$  are tightly clustered between  $-1$  and  $+1$  (variance ( $\sigma^2$ ) between 0.23 and 0.28) with a slightly positive bias, indicating that within our measurement variability the  $\text{NH}_3$  enhancements for all single points could be explained by traffic emissions, in the three urban areas. As shown by the spatial distributions of  $R/U$ , there are only few points in each city with  $R/U \leq -2$  (i.e.  $\text{NH}_3$  not fully explained by traffic) and none with  $R/U \geq 2$  (i.e.  $\text{NH}_3$  from traffic overestimated). Moreover, the positive  $R/U$  values are mostly found in areas with low  $\text{NH}_3$  concentrations (indicated with the marker size in Fig. 6). The points with negative  $R/U$  might be related to the presence of additional sources of  $\text{NH}_3$ , e.g. industrial plants, waste containers, and emissions from agriculture.

Although such point sources are in general very hard to assess, we found evidence that the unexplained  $\text{NH}_3$  in the city suburban area south-west of Tartu was related with cowsheds emissions, which was supported by enhancements in  $\text{CH}_4$  concentrations (see Fig. S21).

Although we demonstrate that in the three cities traffic dominates the urban increments of  $\text{NH}_3$ , the maximum enhancements of  $\text{NH}_3$  in the traffic areas are of the same order or lower than the background concentrations (i.e. ( $P_{75}$ - $P_{05}$ ) of 3.4, 1.8 and 3.0 ppb compared to  $P_{05}$  of 9.3, 4.7 and 3.2 ppb in Zurich, Tartu and Tallinn, respectively). Thus, the background concentrations remain the dominant fraction of  $\text{NH}_3$  in all cases (especially in Zurich and Tartu) and need to be further investigated. By fitting the  $\text{NH}_3$  background concentrations using the HOA and the traffic EFs, we find that traffic can explain  $9.8 \pm 9.6\%$  of the  $\text{NH}_3$  background in Zurich,  $7.7 \pm 18.0\%$  in Tartu, and as much as  $23.8 \pm 26.1\%$  in Tallinn, as shown in Fig. S22. To estimate the uncertainties of the traffic contribution to the  $\text{NH}_3$  background we considered the variability of the HOA background (estimated as the standard deviation of the HOA  $P_{05}$  obtained with the different PMF bootstrap runs) and of the EFs (i.e. the standard deviation of the event-based EFs). Note that this approach considers the deposition processes of  $\text{NH}_3$  to be negligible compared to the dilution of both HOA and  $\text{NH}_3$ . The unexplained  $\text{NH}_3$  background concentrations are most probably related to the regional background of  $\text{NH}_3$ , which is expected to be dominated by agricultural emissions.

Considering both the enhancements ( $P_{75}$ - $P_{05}$ ) in the cities and its contribution to the background concentrations, traffic explains  $33.9 \pm 7.0\%$ ,  $33.3 \pm 13.0\%$  and  $60.7 \pm 13.5\%$  of the total  $\text{NH}_3$  measured in Zurich, Tartu, and Tallinn, respectively. Significant spatial differences in the traffic contributions to  $\text{NH}_3$  emissions are also observed in the inventories compiled for the EURODELTA-III modelling inter-comparison exercise by INERIS at  $0.25^\circ \times 0.25^\circ$  resolution for the year 2009 (Bessagnet et al., 2016; Ciarelli et al., 2016), as shown in Fig. S23. Specifically, the traffic contribution to  $\text{NH}_3$  emissions is on average 11.5% for the cells that include Zurich (6.5% in the cell south of Zurich and 16.5% in the cell north of Zurich), 5.5% for the cells that include Tartu (6.8% in the cell south of Tartu and 4.2% in the cell north of Tartu), and 43.3% for the cell that includes Tallinn. Considering the city-coverage in the cells of interest and our evaluation of the traffic contributions to the background concentrations and urban increments of  $\text{NH}_3$  for the three measurement locations, we can roughly estimate from our measurements a contribution of traffic to  $\text{NH}_3$  emissions of  $13.0 \pm 8.4\%$ ,  $8.9 \pm 17.2\%$  and  $32.7 \pm 16.0\%$  for the cells that include Zurich, Tartu, and Tallinn, respectively. As shown in Fig. S22 these estimates compare fairly well with the cell averages of the emission inventory.

## 5. Conclusions

In this work we combine measurements of  $\text{NH}_3$ ,  $\text{CO}_2$ , eBC and the chemical composition of the NR-PM<sub>2.5</sub> (measured by AMS) to identify and characterize the major sources of  $\text{NH}_3$  and their distributions in three European cities: Zurich (Switzerland), Tartu (Estonia) and Tallinn (Estonia). The use of a heated line with an auxiliary flow minimized the adsorption of  $\text{NH}_3$  on the inlet walls, significantly reducing the response and recovery times of the  $\text{NH}_3$  measurement. In addition, a detailed characterization of the system response and recovery times was used to deconvolve the  $\text{NH}_3$  signal from the remaining adsorption-induced hysteresis, enabling a quantitative characterization of  $\text{NH}_3$  point sources with a mobile sampling platform.

The background concentrations (defined as 5th percentile,  $P_{05}$ ) of  $\text{NH}_3$  ranged between 2 and 19 ppb, with higher levels observed in Zurich (on average 9.3 ppb, compared to 4.7 ppb in Tartu and 3.2 ppb in Tallinn) probably due to more intense agricultural activity. In all three locations,  $\text{NH}_3$  was strongly enhanced in the traffic areas of the city, and its spatial distribution was consistent with those of HOA, eBC and  $\text{CO}_2$ . Average enhancements ( $P_{75} - P_{05}$ ) of 3.4, 1.8 and 3.0 ppb of

NH<sub>3</sub> were measured in the traffic areas in Zurich, Tartu and Tallinn, respectively, representing an enhancement of 36.6, 38.3 and 93.8% over the average background concentrations.

Although the levels of organic aerosols from biomass burning and traffic are comparable in all three locations, traffic clearly dominates the increments of NH<sub>3</sub>, equivalent black carbon (eBC) and carbon monoxide (CO). Traffic EFs of NH<sub>3</sub>, eBC, HOA and CO were estimated using measurements in urban areas highly influenced by traffic, as well as tunnels near Zurich, and were used to characterize the composition of the traffic fleet in the three cities. A similar gasoline:diesel share was estimated for the three locations (gasoline vehicles representing around 44% of the total fleet in Zurich, 50% in Tartu and 33% in Tallinn), but a newer vehicle fleet yields lower EFs in Zurich than Tartu or Tallinn. Based on the retrieved EFs, traffic fully explained the NH<sub>3</sub> enhancements in the three cities, and up to 8–24% of the background concentrations, which are hypothesized to result from agricultural activities. Considering the traffic contributions to the background and the city enhancement of NH<sub>3</sub>, we estimate that 33–61% of the NH<sub>3</sub> measured in the three cities is related to traffic emissions. These results compare fairly well with the available emission inventories for the three cities.

## Acknowledgments

This work was carried out in the framework of the public procurement “Determination of Chemical Composition of Atmospheric Gases and Aerosols in Estonia” of the Estonian Environmental Research Centre (Reference number: 146623), funded by the Estonian–Swiss cooperation program “Enforcement of the surveillance network of the Estonian air quality: Determination of origin of fine particles in Estonia”. The authors would like to thank Picarro Inc., particularly Mr. John Hoffnagle and Mr. Derek Fleck, for the detailed information regarding possible interferences in the NH<sub>3</sub> analyzer. We also acknowledge the support of the Swiss National Science Foundation (IZERZO 142146) and the funding for the measurements in Zurich by the Federal Office for the Environment (FOEN) in Switzerland. Jay G. Slowik acknowledges the support of the Swiss National Science Foundation (starting grant no. BSSG10 155846).

## Appendix A. Supplementary data

Supplementary data related to this article can be found at <http://dx.doi.org/10.1016/j.atmosenv.2017.11.030>.

## References

- Alves, C.A., Calvo, A.I., Lopes, D.J., Nunes, T., Charron, A., Goriaux, M., Tassel, P., Perret, P., 2013. Emissions of Euro 3–5 passenger cars measured over different driving cycles. *Int. J. Environ. Chem. Ecol. Geophys. Eng.* 7, 294–297. <http://dx.doi.org/10.13140/2.1.1995.1048>.
- Alves, C.A., Lopes, D.J., Calvo, A.I., Evtuyugina, M., Rocha, S., Nunes, T., 2015. Emissions from light-duty diesel and gasoline in-use vehicles measured on chassis dynamometer test cycles. *Aerosol Air Qual. Res.* 15, 99–116. <http://dx.doi.org/10.4209/aaqr.2014.01.0006>.
- André, M., Joumard, R., Vidon, R., Tassel, P., Perret, P., 2006. Real-world European driving cycles, for measuring pollutant emissions from high- and low-powered cars. *Atmos. Environ.* 40, 5944–5953. <http://dx.doi.org/10.1016/j.atmosenv.2005.12.057>.
- Bessagnet, B., Pirovano, G., Mircea, M., Cuvelier, C., Aulinger, A., Calori, G., Ciarelli, G., Manders, A., Stern, R., Tsyro, S., García Vivanco, M., Thunis, P., Pay, M.-T., Colette, A., Couvidat, F., Meleux, F., Rouil, L., Ung, A., Aksoyoglu, S., Baldasano, J.M., Bieser, J., Briganti, G., Cappelletti, A., D'Isidoro, M., Finardi, S., Kranenburg, R., Silibello, C., Carnevale, C., Aas, W., Dupont, J.-C., Fagerli, H., Gonzalez, L., Menut, L., Prévôt, A.S.H., Roberts, P., White, L., 2016. Presentation of the EURODELTA III inter-comparison exercise – evaluation of the chemistry transport models' performance on criteria pollutants and joint analysis with meteorology. *Atmos. Chem. Phys.* 16, 12667–12701. <http://dx.doi.org/10.5194/acp-16-12667-2016>.
- Bobbink, R., Hicks, K., Galloway, J., Spranger, T., Alkemade, R., Ashmore, M., Bustamante, M., Cinnerby, S., Davidson, E., Dentener, F., Emmett, B., Erismann, J.W., Fenn, M., Gilliam, F., Nordin, A., Pardo, L., Vries, W., 2010. Global assessment of nitrogen deposition effects on terrestrial plant diversity: a synthesis. *Ecol. Appl.* 20, 30–59. <http://dx.doi.org/10.1890/08-1140.1>.
- Bouwman, A.F., Lee, D.S., Asman, W.A.H., Dentener, F.J., Van der Hoek, K.W., Olivier, J.G.J., 1997. A global high resolution emission inventory for ammonia. *Glob. Biogeochem. Cycles* 11, 561–587.
- Bukowiecki, N., Dommén, J., Prévôt, A.S.H., Richter, R., Weingartner, E., Baltensperger, U., 2002. A mobile pollutant measurement laboratory: measuring gas phase and aerosol ambient concentrations with high spatial and temporal resolution. *Atmos. Environ.* 36, 5569–5579. [http://dx.doi.org/10.1016/S1352-2310\(02\)00694-5](http://dx.doi.org/10.1016/S1352-2310(02)00694-5).
- Canonaco, F., Crippa, M., Slowik, J.G., Baltensperger, U., Prévôt, A.S.H., 2013. SoFi, an IGOR-based interface for the efficient use of the generalized multilinear engine (ME-2) for the source apportionment: ME-2 application to aerosol mass spectrometer data. *Atmos. Meas. Tech.* 6, 3649–3661. <http://dx.doi.org/10.5194/amt-6-3649-2013>.
- Carslaw, D.C., Rhys-Tyler, G., 2013. New insights from comprehensive on-road measurements of NO<sub>x</sub>, NO<sub>2</sub> and NH<sub>3</sub> from vehicle emission remote sensing in London, UK. *Atmos. Environ.* 81, 339–347. <http://dx.doi.org/10.1016/j.atmosenv.2013.09.026>.
- Ciarelli, G., Aksoyoglu, S., Crippa, M., Jimenez, J.L., Nemitz, E., Sellegri, K., Äijälä, M., Carbone, S., Mohr, C., O'Dowd, C., Poulain, L., Baltensperger, U., Prévôt, A.S.H., 2016. Evaluation of European air quality modelled by CAMx including the volatility basis set scheme. *Atmos. Chem. Phys.* 16, 10313–10332. <http://dx.doi.org/10.5194/acp-16-10313-2016>.
- Durbin, T.D., Wilson, R.D., Norbeck, J.M., Miller, J.W., Huai, T., Rhee, S.H., 2002. Estimates of the emission rates of ammonia from light-duty vehicles using standard chassis dynamometer test cycles. *Atmos. Environ.* 36, 1475–1482. [http://dx.doi.org/10.1016/S1352-2310\(01\)00583-0](http://dx.doi.org/10.1016/S1352-2310(01)00583-0).
- Drinovec, L., Mocnik, G., Zotter, P., Prevot, A.S.H., Ruckstuhl, C., Coz, E., Rupakheti, M., Sciare, J., Müller, T., Wiedensohler, A., Hansen, A.D.A., 2015. The “dual-spot” Aethalometer: an improved measurement of aerosol black carbon with real-time loading compensation. *Atmos. Meas. Tech.* 8, 1965–1979. <http://dx.doi.org/10.5194/amt-8-1965-2015>.
- Elser, M., Bozzetti, C., El-Haddad, I., Maasikmets, M., Teinmaa, E., Richter, R., Wolf, R., Slowik, J.G., Baltensperger, U., Prévôt, A.S.H., 2016. Urban increments of gaseous and aerosol pollutants and their sources using mobile aerosol mass spectrometry measurements. *Atmos. Chem. Phys.* 16, 7117–7134. <http://dx.doi.org/10.5194/acp-16-7117-2016>.
- Fangmeir, A., Hadwiger-Fangmeir, A., Van der Eerden, L.J.M., Jager, H.J., 1994. Effects of atmospheric ammonia on vegetation – a review. *Environ. Pollut.* 86, 43–82. [http://dx.doi.org/10.1016/0269-7491\(94\)90008-6](http://dx.doi.org/10.1016/0269-7491(94)90008-6).
- Heeb, N.V., Forss, A.M., Brühlmann, S., Lüscher, R., Saxer, C.J., Hug, P., 2006. Three-way catalyst-induced formation of ammonia: velocity- and acceleration-dependent emission factors. *Atmos. Environ.* 40, 5986–5997. <http://dx.doi.org/10.1016/j.atmosenv.2005.12.035>.
- Huai, T., Durbin, T.S.D., Waynemiller, J., Pisano, J.T., Sauer, C.G., Rhee, S.H., Norbeck, J.M., 2003. Investigation of NH<sub>3</sub> emissions from new technology vehicles as a function of vehicle operating conditions. *Environ. Sci. Technol.* 37, 4841–4847. <http://dx.doi.org/10.1021/es030403+>.
- Huai, T., Durbin, T.D., Younglove, T., Scora, G., Barth, M., Norbeck, J.M., 2005. Vehicle specific power approach to estimating on-road NH<sub>3</sub> emissions from light-duty vehicles. *Environ. Sci. Technol.* 39, 9595–9600. <http://dx.doi.org/10.1021/es050120c>.
- Huang, C., Lou, D., Hu, Z., Feng, Q., Chen, Y., Chen, C., Tan, P., Yao, D., 2013. A PEMS study of the emissions of gaseous pollutants and ultrafine particles from gasoline- and diesel-fueled vehicles. *Atmos. Environ.* 77, 703–710. <http://dx.doi.org/10.1016/j.atmosenv.2013.05.059>.
- Kirkby, J., Curtius, J., Almeida, J., Dunne, E., Duplissy, J., Ehrhart, S., Franchin, A., Gagné, S., Ickes, L., Kürten, A., Kupc, A., Metzger, A., Riccobono, F., Rondo, L., Schobesberger, S., Tsagkogeorgas, G., Wimmer, D., Amorim, A., Bianchi, F., Breitenlechner, M., David, A., Dommén, J., Downard, A., Ehn, M., Flagan, R.C., Haider, S., Hansel, A., Hauser, D., Jud, W., Junninen, H., Kreissl, F., Kvashin, A., Laaksonen, A., Lehtipalo, K., Lima, J., Lovejoy, E.R., Makhmutov, V., Mathot, S., Mikkilä, J., Minginette, P., Mogo, S., Nieminen, T., Onnela, A., Pereira, P., Petäjä, T., Schnitzhofer, R., Seinfeld, J.H., Sipilä, M., Stozhkov, Y., Stratmann, F., Tomé, A., Vanhanen, J., Viisanen, Y., Vrtala, A., Wagner, P.E., Walther, H., Weingartner, E., Wex, H., Winkler, P.M., Carslaw, K.S., Worsnop, D.R., Baltensperger, U., Kulmala, M., 2011. Role of sulphuric acid, ammonia and galactic cosmic rays in atmospheric aerosol nucleation. *Nature* 476, 429–433. <http://dx.doi.org/10.1038/nature10343>.
- Krupa, S.V., 2003. Effects of atmospheric ammonia (NH<sub>3</sub>) on terrestrial vegetation: a review. *Environ. Pollut.* 124, 179–221. [http://dx.doi.org/10.1016/S0269-7491\(02\)00434-7](http://dx.doi.org/10.1016/S0269-7491(02)00434-7).
- Lenschow, P., Abraham, H.J., Kutzner, K., Lutz, M., Preuß, J.D., Reichenbächer, W., 2001. Some ideas about the sources of PM<sub>10</sub>. *Atmos. Environ.* 35 (Suppl. 1), S23–S33. [http://dx.doi.org/10.1016/S1352-2310\(01\)00122-4](http://dx.doi.org/10.1016/S1352-2310(01)00122-4).
- Lopes, M., Serrano, L., Ribeiro, L., Cascão, P., Pires, N., Rafael, S., Tarelho, L., Monteiro, A., Nunes, T., Evtuyugina, M., Nielsen, O.J., Gameiro da Silva, M., Miranda, A.I., Borrego, C., 2014. Emissions characterization from EURO 5 diesel/biodiesel passenger car operating under the new European driving cycle. *Atmos. Environ.* 84, 339–348. <http://dx.doi.org/10.1016/j.atmosenv.2013.11.071>.
- May, A.A., Nguyen, N.T., Presto, A.A., Gordon, T.D., Lipsky, E.M., Karve, M., Gutierrez, A., Robertson, W.H., Zhang, M., Brandon, C., Chang, O., Chen, S., Cicero-Fernandez, P., Dinkins, L., Fuentes, M., Huang, S.-M., Ling, R., Long, J., Maddox, C., Masetti, J., McCauley, E., Miguel, A., Na, K., Ong, R., Pang, Y., Rieger, P., Sax, T., Truong, T., Vo, T., Chattopadhyay, S., Maldonado, H., Maricq, M.M., Robinson, A.L., 2014. Gas- and particle-phase primary emissions from in-use, on-road gasoline and diesel vehicles. *Atmos. Environ.* 88, 247–260. <http://dx.doi.org/10.1016/j.atmosenv.2014.01.046>.
- Martin, N.A., Ferracci, V., Cassidy, N., Hoffnagle, J.A., 2016. The application of a cavity ring-down spectrometer to measurements of ambient ammonia using traceable primary standard gas mixtures. *Appl. Phys. B* 122, 219. <http://dx.doi.org/10.1007/s00340-016-6486-9>.

- Paatero, P., Tapper, U., 1994. Positive matrix factorization: a nonnegative factor model with optimal utilization of error estimates of data values. *Environmetrics* 5, 111–126.
- Perrino, C., Catrambone, A., Di Menno Di Bucchianico, A., Allegrini, I., 2002. Gaseous ammonia in the urban area of Rome, Italy and its relationship with traffic emissions. *Atmos. Environ.* 36, 5385–5394. [http://dx.doi.org/10.1016/S1352-2310\(02\)00469-7](http://dx.doi.org/10.1016/S1352-2310(02)00469-7).
- Reche, C., Viana, M., Pandolfi, M., Alastuey, A., Moreno, T., Amato, F., Ripoll, A., Querol, X., 2012. Urban NH<sub>3</sub> levels and sources in a Mediterranean environment. *Atmos. Environ.* 57, 153–164. <http://dx.doi.org/10.1016/j.atmosenv.2012.04.021>.
- Reche, C., Viana, M., Karanasiou, A., Cusack, M., Alastuey, A., Artíñano, B., Revuelta, A., López-Mahía, P., Blanco-Heras, Rodríguez, S., Sánchez de la Campa, A.M., Fernández-Camacho, R., González-Castanedo, Y., Mantilla, E., Tang, Y.S., Querol, X., 2015. Urban NH<sub>3</sub> levels and sources in six major Spanish cities. *Chemosphere* 119, 769–777. <http://dx.doi.org/10.1016/j.chemosphere.2014.07.097>.
- Sandradewi, J., Prévôt, A.S.H., Szidat, S., Perron, N., Alfarra, M.R., Lanz, V.A., Weingartner, E., Baltensperger, U., 2008. Using aerosol light absorption measurements for the quantitative determination of wood burning and traffic emission contributions to particulate matter. *Environ. Sci. Technol.* 42, 3316–3323. <http://dx.doi.org/10.1021/es702253m>.
- Suarez-Bertoa, R., Zardini, A.A., Astorga, C., 2014. Ammonia exhaust emissions from spark ignition vehicles over the New European Driving Cycle. *Atmos. Environ.* 97, 43–53. <http://dx.doi.org/10.1016/j.atmosenv.2014.07.050>.
- Suarez-Bertoa, R., Astorga, C., 2016. Isocyanic acid and ammonia in vehicle emissions. *Transp. Res. D-Tr E* 49, 259–270. <http://dx.doi.org/10.1016/j.trd.2016.08.039>.
- Sutton, M.A., Dragosits, U., Tang, Y.S., Fowler, D., 2000. Ammonia emissions from non-agricultural sources in the UK. *Atmos. Environ.* 34, 855–869. [http://dx.doi.org/10.1016/S1352-2310\(99\)00362-3](http://dx.doi.org/10.1016/S1352-2310(99)00362-3).
- Sutton, M.A., Reis, S., Riddick, S.N., Dragosits, U., Nemitz, E., Theobald, M.R., Tang, Y.S., Braban, C.F., Viero, M., Dore, A.J., Mitchell, R.F., Wanless, S., Daunt, F., Fowler, D., Blackall, T.D., Milford, C., Flechard, C.R., Loubet, B., Massad, R., Cellier, P., Personne, E., Coheur, P.F., Clarisse, L., Van Damme, M., Ngadi, Y., Clerbaux, C., Ambelas Skjøth, C., Geels, C., Hertel, O., Wichink Kruit, R.J., Pinder, R.W., Bash, J.O., Walker, J.T., Simpson, D., Horváth, L., Misselbrook, T.H., Bleeker, A., Dentener, F., de Vries, W., 2013. Towards a climate-dependent paradigm of ammonia emission and deposition. *Philos. Trans. R. Soc. B* 368, 20130166. <http://dx.doi.org/10.1098/rstb.2013.0166>.
- Zotter, P., Herich, H., Gysel, M., El-Haddad, I., Zhang, Y., Močnik, G., Hüglin, C., Baltensperger, U., Szidat, S., Prévôt, A.S.H., 2017. Evaluation of the absorption Ångström exponents for traffic and wood burning in the Aethalometer based source apportionment using radiocarbon measurements of ambient aerosol. *Atmos. Chem. Phys.* 17, 4229. <https://doi.org/10.5194/acp-17-4229-2017>.